NUMERICAL SIMULATION OF MICROSTRUCTURAL EVOLUTION OF NODULAR CAST IRON - FOR THE CASE OF AUTOMOBILE CRANKSHAFT BY THE CRONING PROCESS

S.-M. Yoo, A. Kleine, A. Ludwig and P.R. Sahm

Giesserei-Institut der RWTH Aachen
Intzestrasse 5, D-52056 Aachen, Germany
e-mail: seung@gi.rwth-aachen.de

Abstract

A simulation model was developed to predict the microstructural evolution during the solidification and the subsequent solid state transformation of nodular cast iron in Fe-C-Si ternary system for an automobile crankshaft by the croning process. In the simulation of the solidification process of nodular cast iron it is assumed that eutectic grains are formed under the eutectic temperature and the growth rate of these eutectic grains are controlled by carbon diffusion through the austenite shell. Carbon and silicon concentrations at any interfaces are calculated from the Fe-C-Si phase diagram obtained from the thermodynamic phase equilibrium calculation tool, ChemApp™. The ferrite growth from the austenitic matrix under the eutectoid temperature was described by modeling carbon diffusion through the ferrite. The corresponding change in carbon solubility in the austenite was considered by using the above mentioned thermodynamic tool. The distribution of temperature, nodule counts, nodule sizes and phase fractions in the casting were calculated. The simulation was compared with experimental results obtained from the croning process.

Modeling of Casting, Welding and Advanced
Solidification Processes VIII
Edited by B.G. Thomas and C. Beckermann
The Minerals, Metals & Materials Society, 1998

Introduction

The casting alloys' mechanical properties depend mainly on the structure of the matrix in the as-cast condition or after heat treatment. In spheroidal graphite cast iron the nodularity of the graphite phase is also very important for the material characteristics. If the microstructural evolution and the phase transformation of the nodular cast iron can be determined by numerical simulation, the mechanical properties of the final material can be predicted. Moreover the calculation of the volume change between the different phases allows the calculation of the residual stresses of castings during the casting process.

After the early work of Oldfield [1] and Wetterfall *et al.* [2], much work has been carried out on the modeling of the solidification and solid state transformation of nodular cast iron [3-5]. Recently the microsegregation of silicon during solidification has been taken into account [6,7]. The solidification of nodular cast iron can be calculated by nucleation and growth of grains in terms of carbon diffusion through austenite shells [2-4,10,11]. The eutectoid transformation of nodular cast iron consists of the transformation of austenite matrix into ferrite and pearlite. It can be predicted on the assumption that the formation rate of ferrite is controlled by the diffusion rate of carbon through the ferrite shell under steady state [4,8-11]. The fraction of pearlite formed in ductile iron can be calculated by a modified Avrami equation [12,13]. The object of this work is to simulate the microstructural evolution of nodular cast iron during the croning process based on the present models.

Mathematical Model

The macroscopic heat transport equation is solved with an in-house FD-code, taking into account a temperature-dependent heat-transfer coefficient between mould and metal. The release of enthalpy due to a phase transition is described by a micro-model, both for solidification and for the solid-state reaction. This enthalpy release is taken into account on the macro-level by changing the temperature at the corresponding nodal point without back-iteration. To ensure that the temperature evolution is still reliably predicted, a quite small time step ($\Delta t \leq 0.05$ s) has been used. The micro-model is examined at those nodal points of the FD-program where the temperature dropped into the corresponding temperature range.

To describe the solidification of nodular cast iron, it is assumed that eutectic grains (*i.e.* graphite spheres enveloped by austenite shells) are formed as the temperature decreases below the eutectic temperature. Thus no primary austenite and no pure graphite spheres are considered to grow even when the concentration of the alloy is slightly off-eutectic. With a nucleation rate which is assumed to be related to the undercooling by a power law function [3,10,11], the numbers of graphite nodules is considered to increase at each time step until the cooling curve has reached its minimum.

The eutectic grain is thought to start growing with an initial graphite radius of 1.0 μm and an austenite shell of 0.2 μm in thickness [3]. The growth of the graphite sphere as well as of the austenite shell is described by the analytical expressions given in ref. [2-4,10,11]. These expressions assume that (i) carbon diffusion is the most relevant growth mechanism, (ii) a quasi-steady-state profile of carbon in the austenite shell is present, and (iii) the global mass balance is assured. Both growth rates are proportional to the carbon gradient in the austenite shell, and inversely proportional to the concentration change at the corresponding interface.

As the concentrations at the graphite/austenite and at the austenite/liquid interfaces are temperature-dependent, assumptions on the thermodynamics of the system had to be made. Additionally in this work the well-known effect of Si on the eutectic and eutectoid temperature should be taken into account. Therefore we have considered a Gulliver-Scheil-like (negative) segregation of Si. The necessary thermodynamical information was then taken from thermodynamic equilibrium calculations for the Fe-C-Si-system. These calculations were performed with the commercial software tool ChemApp™ [14], which is a FORTRAN library for calculating thermodynamic equilibria in complex systems based on the CALPHAD method.

The evolution of solid fraction was calculated locally from the product of the actual nucleation density and the actual volume of the eutectic grains. In the event of new grains being formed besides those already existing, an average solid fraction was calculated by averaging the different volumes of the new and the old grains weighted by the corresponding grain density. For solid fractions larger than 0.5 the impingement of the grains was examined by modifying the austenite growth rate with the weighting factor $\left((1-f_s)/0.5\right)^{2/3}$ [3].

From the micro-model for the solidification of nodular cast iron, the density of graphite nodules and the volume fraction of graphite and austenite at every position in the casting were evaluated. For comparison of the calculated graphite density with experimental results, the volumetric value of the density was translated into an area value by using Owadano's equation in ref. [15].

The eutectoid reaction is modeled by assuming that the ferrite starts growing at the graphite/austenite interface. For the growth rate of the ferrite into the austenite and the graphite into the ferrite, again analytical expressions from the literature [4,8-11] are used. Similar to the case of solidification, these expressions assume that (i) carbon diffusion is the most relevant growth mechanism, (ii) a quasi-steady-state profile of carbon in the ferrite shell is present, (iii) the concentration gradient in the austenite has already disappeared and (iv) the global mass balance is assured. Both growth rates are again proportional to the carbon gradient (now in the ferrite shell), and inversely proportional to the concentration change at the corresponding interface.

Table I. Thermo-physical data used in the calculation

Density, kg/m^3		Latent heat, J/kg	
metal:	7200	fusion:	2.1×10^5
mould:	1500	formation (ferrite):	5.8×10^4
Specific heat, J/(kg K)		formation (pearlite):	7.58×10^4
metal:	$415.3+0.23307 \cdot T$	Partition coefficient	
mould:	1092	silicon:	1.09
Thermal conductivity, W/(m K)		Initial temperature, K	
metal:	$48.68-0.02547 \cdot T$	melt:	1660
mould:	0.669	mould:	300

As in practice austenite is transformed not only into ferrite but also into pearlite, this reaction is also examined. The transformed amount of pearlite from austenite is described by an Avrami equation [12] with temperature-dependent Avrami coefficients (prefactor and exponent). These coefficients were determined at each temperature from the "start" and "end" of isotransformation curves on the TTT-diagram taken from ref. [17]. To calculate the phase

change during continuous cooling, the Avrami equation was modified by applying the additivity rule [13,18,19].

The thermo-physical data used in the simulation are listed in Table I.

Experimental Procedures

The automobile crankshaft relevant for this work is produced by the croning process. Fig. 1 shows schematically the shape of the casting. To prevent cracking of the shell mould during form filling and solidification, the shell mould was stabilized by using green sand.

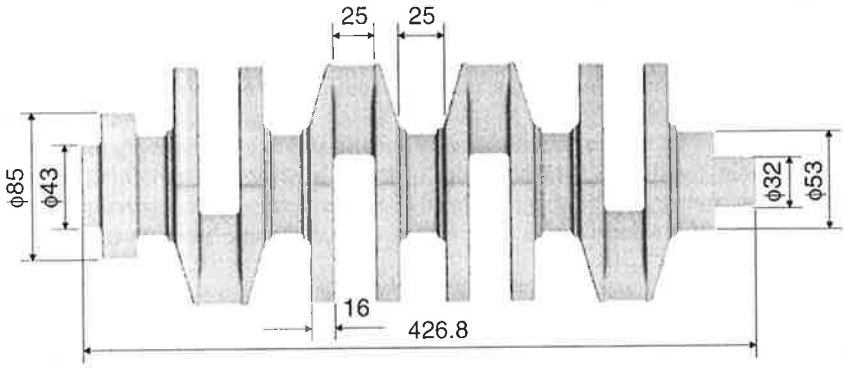

Fig. 1 Schematic of the casting. Dimensions are given in mm.

A batch of pig iron, steel and ferro-silicon was melted in a middle-frequency induction furnace. It was treated with 0.5 kg FeSiMg10 alloy for spheroidization. After treatment and inoculation the melt containing 77.8 ppm Bi was poured into a shell mould with a pouring temperature of 1390°C. The chemical composition of the nodular cast iron produced is listed in Table II. This alloy system is chosen because it reveals only a small deviation from the Fe-C-Si ternary system, the basis of our calculations. The addition of bismuth promotes the formation of a pearlitic microstructure. Since bismuth is known to cause degeneration of the spheroidal graphite formation, cerium was used to avoid this effect.

Table II. Chemical composition of the nodular cast iron (wt %)

Fe	C	Si	Cu	Ni	Mn	P	S	Cr	Mg
Bal.	3.62	2.43	1.13	0.2	0.09	0.021	0.007	0.035	0.037

To record the cooling curves, type B thermocouples (Pt-30%Rh and Pt-6%Rh) 0.2 mm in diameter were implanted at four locations in the casting. An image analysis system was used to determine the nodule counts, nodule sizes and the relative amounts of ferrite and pearlite in the matrix.

Results and Discussions

Cooling behavior

Fig. 2 shows the experimental and calculated cooling curves at different positions (at TC2 and TC3). In these calculations the influence of the form filling were not considered, *i.e.*, the temperature distribution was initially set at the constant pouring temperature. Experimentally the melt already cools during pouring into the mould. Thus at the beginning of cooling the calculated temperatures are higher than those measured. However, the eutectic temperature calculated by ChemApp™ agrees well with the experimental measurements.

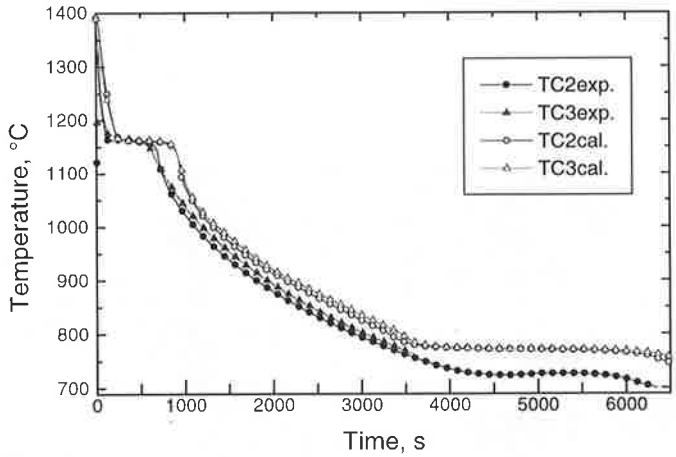

Fig. 2 Experimental and calculated cooling curves in the casting. (positions TC2 and TC3 as depicted in Fig. 3)

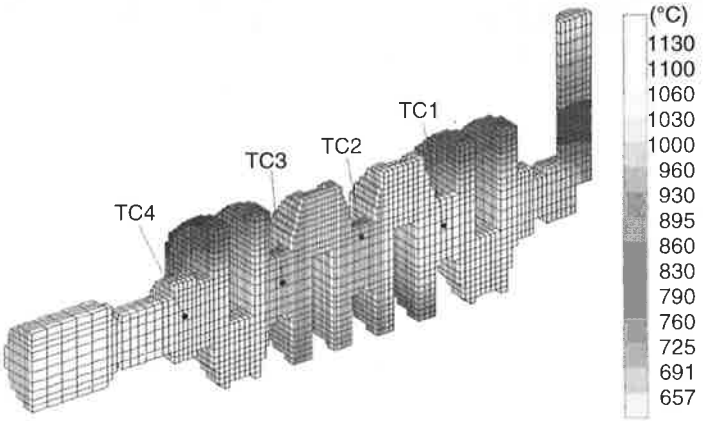

Fig. 3 Temperature field of the casting, 600 seconds after pouring.

The calculated cooling curves did not agree closely with the experiments during the eutectoid transformation. The eutectoid temperature calculated by ChemApp™ deviates from the experimental results, because the influence of copper on the eutectoid transformation was not taken into account in the calculation. It is well known that copper is a pearlite promoter and decreases the eutectoid temperature. The calculated temperature field 600 seconds after

"pouring" is shown in Fig. 3. The middle part of the casting, especially the center line, is still liquid.

Nodule counts and sizes

The microstructures of the nodular cast iron produced by the croning process consist of graphite nodules surrounded by ferrite and pearlite as shown in Fig. 4. In nodular cast iron nodule count is one of the most important parameters. Experimentally measured nodule counts at two positions in the casting and calculated results are shown in Fig. 5. The nodule count near the surface (at TC2) was 2.6×10^4 /cm^2 experimentally and 1.8×10^4 /cm^2 on calculation. At position TC3 it was 2.1×10^4 /cm^2 experimentally and 1.6×10^4 /cm^2 on calculation. Fig. 6 shows the comparison of the calculation and the experiment of the radii of graphite nodules at different positions. The average radius near the surface is 12.6 μ experimentally, 15.2 μ on calculation.

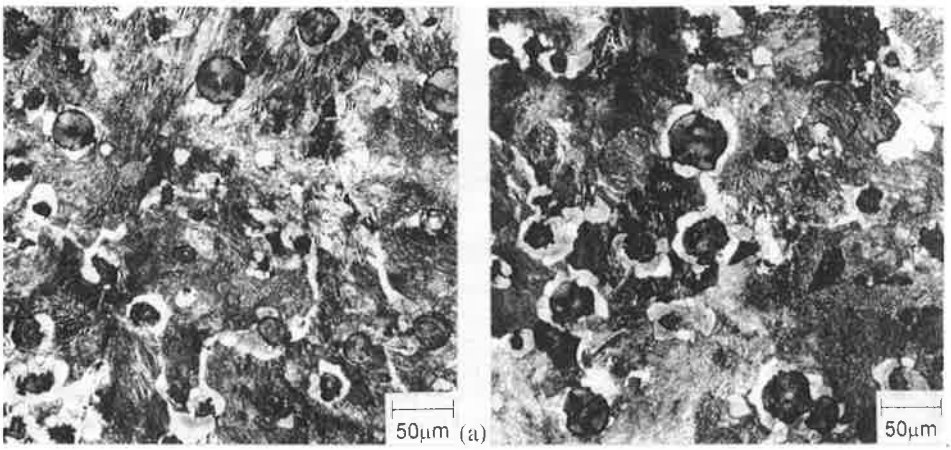

Fig. 4 Microstructure of nodular cast iron near the surface (position TC2 as shown in Fig. 3) (a) and at the center of the casting (position TC3 as shown in Fig 3) (b) (x 200, 3% NHO_3 etched).

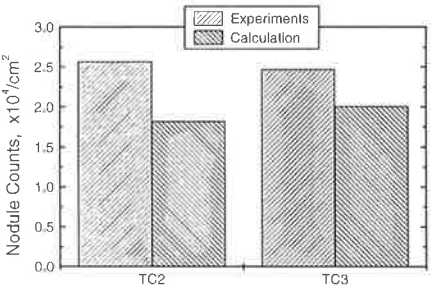

Fig. 5 Nodule counts by the experiment and the calculation.

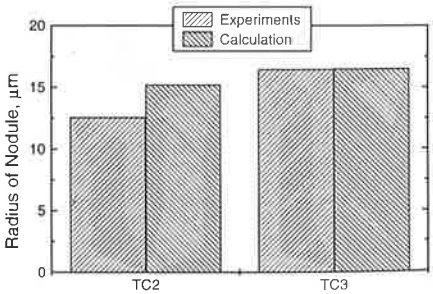

Fig. 6 Nodule sizes (radii) by the experiment and the calculation.

The calculated nodule counts and nodule sizes agree well with the experimental results. The change of the calculated mean nodule sizes at different locations of the casting and the

corresponding nodule counts during the solidification are shown in Fig. 7. The differences of nodule counts and nodule sizes between the middle of the casting (TC 3) and near the surface (TC 2) were found to be small. The calculated change in graphite radii during the eutectoid transformation was negligible.

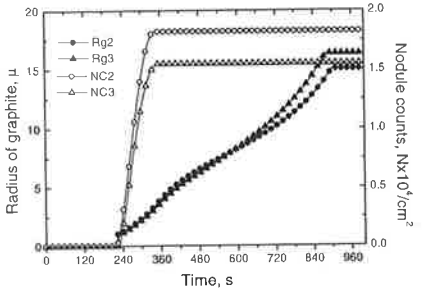

Fig. 7 The calculated change of nodule counts and nodule sizes (at TC2 and TC3).

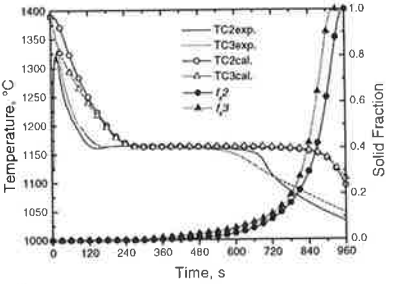

Fig. 8 Experimental and calculated cooling curves as in Fig. 2 with the corresponding evolution of solid fraction.

Amount of phases

The evolution of solid fraction during solidification at two different positions within the casting is shown in Fig. 8.

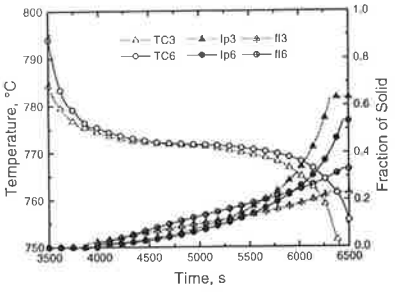

Fig. 9 Calculated curves of transformed ferrite and pearlite (at TC2 and TC3)

At the position labeled with TC3 in Fig. 3, the average fraction of graphite is 13 %, the ferrite fraction is 21 % and the pearlite fraction is 76 % at room temperature. The calculated evolution of the fractions of ferrite and pearlite at TC3 in the casting are shown in Fig.9. The fraction of ferrite by the calculation was about 23.0 % and that of pearlite about 63.2 %. In the simulation of eutectoid transformation the influence of copper was not taken into account, although copper decreases the eutectoid temperature and prevents carbon diffusion to graphite.

Conclusions

Numerical work was carried out to simulate the microstructural evolution of austenite and spheroidal graphite during the solidification process of the Fe-C-Si system with Si inverse segregation, and the eutectoid transformation during subsequent cooling in nodular cast irons. In the croning process nodule counts and nodule sizes at the different locations in the casting were very similar and the calculated results agreed well with the experimental results. When the shape of the casting is complicated, as in the case of a crankshaft, the simulation of form filling becomes more important for the calculation of the initial temperature field in the casting and the early stage of the solidification. The calculation of the eutectoid transformation in this work should be more improved by examing the effect of alloying elements such as copper and nickel on transformation.

Acknowledgement

One of the authors (S.-M. Yoo) gratefully acknowledge the financial support from "Deutscher Akademischer Austauschdienst" for his work.

References

1. W. Oldfield, "A Quantitative Approach to Casting Solidification: Freezing of Cast Iron," Trans. of the ASM, 59, (1966), 945-961.
2. S. E. Wetterfal, H. Fredriksson and M. Hillert, "Solidification Process of Nodular Cast Iron," J. Iron and Steel Institute, (1972), 323-333.
3. K. -C. Su and I. Ohnaka, "Computer Simulation of Solidification of Nodular Cast Iron," Mat. Res. Soc. Symp. Proc., 34, (1985), 181-189.
4. S. Chang, D. Shangguan and D. M. Stefanescu, "Modeling of the Liquid/Solid and the Eutectoid Phase Transformations in Spheroidal Graphite Cast Iron," Met. Trans., 23A, (1992), 1333-1346.
5. J. Lacaze and G. Lesoult, "Modelling the Formation of Microstructures: the Example of Spheroidal Graphite Cast Iron," Advanced casting and solidification Technology, eds. H. Kleemola and K. Pithan, (1994), 5-34.
6. E. Lundbäck, "On Modeling and Computer Simulation of Eutectic Solidification," Thesis, KTH, Stockholm, Sweden, (1991).
7. A. Almansour, K. Matsugi, T. Hatayama and O. Yanagisawa, "Simulation Solidification of Spheroidal Graphite Cast Iron of Fe-C-Si System," Mat. Trans. JIM, 36, (1995), 1487-1495.
8. D. Venugopalan, "A Kinetic Model of the $\gamma \rightarrow \alpha$ + Gr Eutectoid Transformation in Spheroidal Graphite Cast Irons," Met. Trans., 21A, (1990), 913-918.
9. M. Wessén and I. L. Svensson, "Modeling of Ferrite Growth in Nodular Cast Iron," Met. and Mat. Trans., 27A, (1996), 2209-2220.
10. S.-M. Yoo, A. Ludwig, K. Moeinipour and P. R. Sahm, "Modeling of *in situ* Heat Treatment in Austempered Ductile Iron," 5th EuroMAT, (1997), 669-672.
11. S.-M. Yoo, A. Ludwig and P.R. Sahm, " Numerical Simulation of Solidification of Nodular Cast Iron in Permanent Moulds," Solidification Processing 1997, (1997), 494-497.
12. M. Avrami, "Kinetics of Phase Change. I," J. Chem. Phy., 7, (1939), 1103-1112 and "Kinetics of Phase Change. II," J. Chem. Phy., 4, (1940), 212-224.
13. P. K. Agarwal and J. K. Brimacombe, "Mathematical Model of Heat Flow and Austenite-Pearlite Transformation in Eutectoid Carbon Steel Rods for Wire," Met. Trans., 12B, (1981), 121-133.
14. G. Eriksson and K. Hack, "ChemSage - A Computer Program for the Calculation of Complex Chemical Equilibria," Met. Trans., 21B, (1990), 1013.
15. T. Owadano, K. Torigoe and I. Kanzak, "The Interrelationship of Solidification Time, Undercooling and the Number of Graphite Nodules in Spheroidal Graphite Iron," Imono, 48, (1976), 563-567.
16. E.Scheil, "Bemerkungen zur Schichtkristallbildung," Zeitschrift für Metallkunde., 34 (1942) 70-72.
17. K. Röhrig and W. Fairhurst, Heat Treatment of Nodular Cast Iron, (Düsseldorf, Germany: Giesserei-Verlag GmbH, 1979), 46-106.
18. E. Scheil, "Anlaufzeit der Austenitumwandlung," Arch. Eisenhüttenwes., 12, (1935), 565-567.
19. M. Umemoto, K. Horiuchi and I. Tamura, "Pearlite Transformation during Continuous Cooling and Its Relation to Isothermal Transformation," Trans. ISIJ, 23, (1983), 690-695.